Article Pre-Print

Dynamic modeling of integrated mixed reforming and nuclear heat systems

Leila Hoseinzade, Thomas A. Adams II*

Department of Chemical Engineering, McMaster University, 1280 Main St W,

Hamilton, Ontario, L8S 4L7, Canada

*Corresponding author: tadams@mcmaster.ca

Abstract

In the previous study, a dynamic and two-dimensional model for a steam methane reforming process integrated with nuclear heat production was developed. It was shown that the integrated HTGR/SMR is an efficient process for applications such as hydrogen production. In this study, it is demonstrated that combining nuclear heat with the mixed of steam and dry reforming process can be a promising option to achieve certain desired H_2/CO ratios for Fischer-Tropsch or other downstream energy conversion processes. The model developed in the previous study is extended to the combined steam and dry reforming process. The resulting model was validated using reported experimental data at non-equilibrium and equilibrium conditions. The dynamic and steady state performance of the integrated mixed reforming of methane and nuclear heat system was studied and it was found that in addition to desired H_2/CO ratios, higher methane conversion and lower CO_2 emissions can be achieved using the proposed design compared to HTGR/SMR system.

Keyword: steam reforming of methane, dry reforming of methane, Dynamic modeling, Syngas, Integrated systems, Nuclear heat.

1. Introduction

Syngas, a mixture of hydrogen and carbon monoxide, is an important feedstock to produce various products such as electricity, methanol, dimethyl ether, ammonia, synthetic fuels by the Fischer-Tropsch (FT) process, and so on[1]. The steam reforming of methane process is a well-established and economical method for syngas production[2, 3] , which yields a hydrogen rich syngas. However, when using steam as the feed, the hydrogen to carbon monoxide ratio is often too high to be used directly for the FT process[4, 5]. CO_2 reforming of methane (also known as dry reforming of methane or DRM) is a potentially attractive method of producing syngas since it

converts captured carbon dioxide (a waste and greenhouse gas (GHG)) into valuable syngas[6, 7]. The resulting syngas from dry reforming has an H_2/CO molar ratio of around 1, which is suitable for the production of dimethyl ether (DME) but too low for FT production. However, due to carbon deposition and rapid catalyst deactivation during the dry reforming reaction, the application is limited in practice[6].

Different catalysts have different potentials for carbon formation in the CO_2 reforming reaction. Many studies investigated the activity and resistance of various catalysts (including noble metals, Ni, and graphite–based catalysts) to carbon deposition in the dry reforming reaction[7, 8]. The results generally demonstrated that in the absence of steam, carbon deposition occurs for all the studied catalyst types, however, noble metal and Ni based catalysts have less selectivity for carbon deposition than graphite[8]. Furthermore, among the noble metals, Ru and Rh have the highest activity the highest resistance to carbon formation[7, 8]. Although, the activities of the Ru and Rh-based catalysts are about ten times larger than the activity of Ni, the latter is still a promising catalyst for industrial applications considering its reasonable performance, low cost, and availability[7, 9].

Due to the catalyst deactivation issue, the dry reforming process has not been commercialized at large scales. However, combined dry and steam reforming processes have been commercialized in several countries[2]. Using steam in the dry reforming feedstock converts higher hydrocarbons (which are often present in natural gas) into H_2 and CO and reduces the risk of carbon deposition[2]. There is a certain minimum amount of steam necessary to prevent carbon deposition which depends on the catalyst type and the CO_2/CH_4 ratio in the feed[2]. Moreover, the H_2/CO ratio of the syngas produced by the combined process is in between that of dry reforming and steam reforming, much closer to the 2.0 ratio required for the FT process.

The steam reforming and water gas shift (WGS) reactions are given as follows[10]:

$$CH_4 + H_2O \rightleftharpoons CO + 3H_2 \left(\Delta H_{r,298k} = 206.3 \frac{kJ}{mol}\right) \quad (1)$$

$$CO + H_2O \rightleftharpoons CO_2 + H_2 \left(\Delta H_{r,298k} = -41.1 \frac{kJ}{mol}\right) \quad (2)$$

$$CH_4 + 2H_2O \rightleftharpoons CO_2 + 4H_2 \left(\Delta H_{r,298k} = 164.9 \frac{kJ}{mol}\right) \quad (3)$$

The dry reforming reaction proceeds as follows[9]:

$$CH_4 + CO_2 \rightleftharpoons 2CO + 2H_2 \left(\Delta H_{r,298k} = 247 \frac{kJ}{mol}\right) \quad (4)$$

All of the dry and steam reforming reactions are highly endothermic and require large amount of heat in order to reach equilibrium.

The SMR reaction mechanism and kinetics are well studied and understood. The well-known kinetic model of this reaction based on the Nickel catalyst was presented using a Langmuir-Hinshelwood type model by Xu and Froment[11]. However, the reaction kinetics and mechanisms of the dry reforming process are still less well known.

Richardson et al. [Richardson] studied the kinetics of the DRM reaction on a Rh/γ-Al_2O_3 catalyst and presented a model based on the Langmuir-Hinshelwood framework and a redox mechanism. Their results showed that for low CO_2/CH_4 ratios there is no carbon deposition at temperatures of 600-800ºC. Bradford et al.[12] investigated the dry reforming reaction on a Ni catalyst with different supports (TiO_2, C, SiO_2 and MgO) and indicated that catalyst activity significantly varies for different supports. They found Ni/MgO to be the most stable and active catalyst between the studied cases. They also developed an expression for the reaction rate for the Ni catalysts based on assuming CH_4 and CH_xO decompositions as the slow kinetic steps[13].

In addition, Olsbye et al.[14] developed a kinetic model for the CO_2 reforming of methane based on the Langmuir-Hinshelwood type equation on the Ni/La/α-Al_2O_3 based catalyst and showed that experimental data is consistent with this type of model. Wang et al.[15] studied the kinetics of the dry reforming reaction over a Ni/γ-Al_2O_3 catalyst and presented a Langmuir-Hinshelwood mechanism similar to Olsbye's model. The results of this study indicated that Ni/γ-Al_2O_3 is an effective catalyst for this reaction and a Langmuir-Hinshelwood equation is a proper model to represent the kinetics of the reaction. Maestri et al.[16] developed a detailed micro-kinetic model for the SMR and DRM reaction kinetics on a Rh/Al_2O_3 catalyst. The results of this study showed that methane activation is the rate determining step of the dry reforming reaction.

Based on Zhao et al.[17] and our survey of the literature, the best kinetic model to describe the combined dry and steam reforming kinetics is the model presented by Park et al.[18]. This kinetic model is a combination of the SMR kinetic model proposed by Xu et al.[11] and dry reforming kinetic model presented by Olsbye et al.[14]. These kinetic models, as briefly explained above, are Langmuir-Hinshelwood type expressions developed for Ni-based catalysts. This study provided

correlations for the equilibrium and reaction coefficients based on lab scale data from a fixed-bed micro reactor. In Park's study, the reaction was under non-equilibrium conditions by using inert solids and high feed flow rate to catalyst ratios. The model also was validated using lab scale experimental data for various ranges of the pressure, temperature and feed flow rates. Their results indicated consistency between the experiments and model prediction[18].

As mentioned earlier, both the dry and steam reforming processes are highly endothermic and energy intensive. Conventionally, reforming tubes are placed inside a furnace and heat is provided by combusting a fuel. In addition, the endothermic reforming process can be combined with exothermic partial oxidation of methane (POM) process to provide the required heat in which high purity oxygen is injected as an additional reagent. However, it has some disadvantages such as forming hot spots in the catalyst which results in catalyst deactivation[19, 20] and the expense of adding an air separation unit to produce the necessary high purity oxygen[18]. Furthermore, either using a furnace or partial oxidation causes large GHG emissions; thus, it is important to investigate alternate sources to reduce total greenhouse gas emissions of the process.

Several researchers studied nuclear energy as an alternate source of heat for the steam reforming process[21-26]. Researchers in Germany and Japan tested the integrated high temperature gas-cooled reactor (HTGR) and SMR processes for hydrogen production at pilot scale and demonstrated that nuclear heat is a safe, clean and economically feasible source of energy to produce hydrogen[21-24]. Khojasteh-Salkuyeh and Adams also showed that by integrating HTGR with SMR process, direct fossil fuel consumption significantly decreases and carbon efficiency increases[25, 26] .

The feasibility and operability of the integrated HTGR/SMR process were demonstrated by pilot scale facilities by research groups in Germany and Japan Atomic Energy Research Institute[21-24]. The dynamic modeling of the process was also developed in the previous work[27] to address the key challenges of the process concerning dynamic behavior, such as start-up, shutdown, and response to disturbances. In the previous work, the dynamic model was developed based on first principles using a multi-scale model, considering phenomena such as gas diffusion inside catalysts[27]. The validity of the model was tested using available data and very few model parameters needed to be fit based on the reported design data. The dynamic and steady state

variations of the key variables of the system were analyzed and it was found that to obtain higher methane conversions, a high steam to methane ratio in the feed is required. This leads to a large H_2/CO ratio which is more suitable for hydrogen production than for FT processes.

Therefore, as mentioned earlier, to obtain lower H_2/CO ratios which is suitable for FT process, mixed reforming process is preferable. The required heat for the MRM process can be provided by high temperature gas-cooled reactors as was previously considered for the SMR process. However, to the best of the authors' knowledge integrating nuclear heat and mixed reforming process has not been investigated.

The purpose of this study is to propose a large scale design for the novel integrated nuclear heat and mixed reforming process. To do this, the dynamic model which was developed in the previous study is extended to the mixed reforming process. The model is based on the conservations of mass, momentum and energy within the system, and common correlations for physical properties, heat and mass transfer coefficients and diffusion. Also, Park's kinetic model for the MRM reactions are applied. The final model (a set of partial differential and algebraic equations, or PDAEs) is implemented and solved using the finite differences method with the gPROMS software package, an equation-oriented modelling and simulation environment. To the best of our knowledge, there is no large scale experimental data on the integrated HTGR/MRM process, so the validity of the model for the mixed reforming process is checked using lab scale data. After verifying the validity of the model, the dynamic and steady state performance of the system is analyzed, as well as its transient behavior in the presence of disturbances. Finally, a sensitivity analysis on the key parameters of the system is accomplished to investigate the system performance in presence of parameter uncertainty. This information was used to develop a final recommended design for the integrated HTGR/MRM reactor.

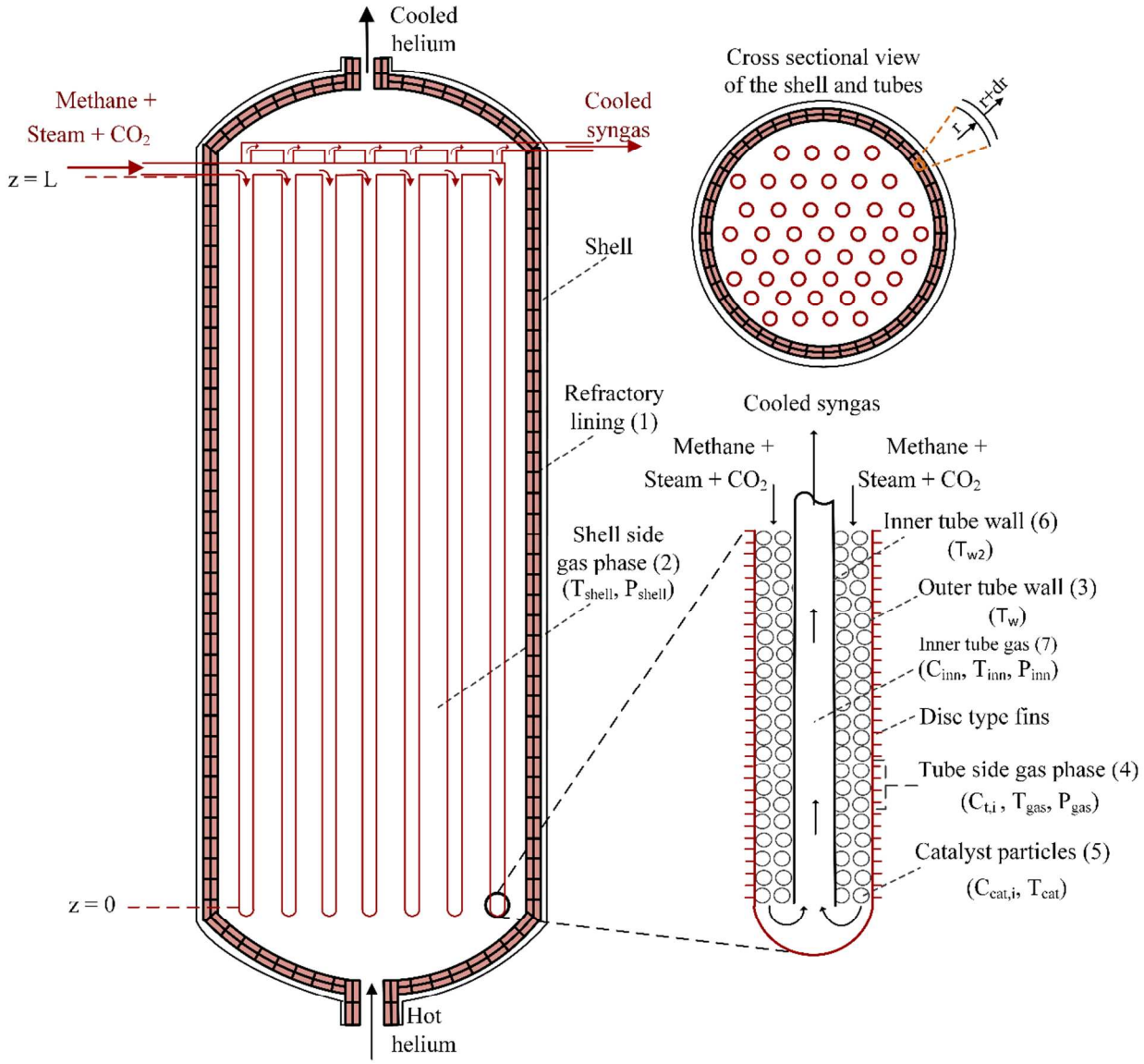

Figure 1. Schematic of integrated HTGR/MRM system. This figure was adapted from the study by Hoseinzade et al.[27].

2. Model development

A schematic of the proposed integrated HTGR/MRM system is shown in Figure 1. The model of this system contains seven sub-models at different scales including (1) refractory lining of the shell, (2) gas phase in the shell side, (3) outer tube wall of the mixed reforming tubes, (4) gas phase in the reforming tubes, (5) catalyst particles which are packed inside the reforming tubes, (6) inner tube wall, and (7) gas phase in the inner tubes. Table 1 briefly describes each sub-model. The model and the assumptions are the same as in the previous study except the reaction kinetics which are presented in section 2.1 below. Key assumptions of the model are given in

Table 2. To avoid repetition, the model equations are not presented here. The only difference between the models is that equations (44)-(63) of the previous study has to be replaced by equations (5)-(27) of this study to represent the MRM reaction kinetics and rates properly. The rest of the model equations are the same and the detailed model equations can be found in the study by Hoseinzade et al.[27].

Table 1. Description of the sub-models.

Sub-model	Description
(1) refractory lining of the shell	Considers the temperature gradient in the axial and radial directions of the refractory lining based on the conductive heat transfer as given by equations (1)-(5) of the study by Hoseinzade et al.[27]
(2) gas phase in the shell side	Considers the concentration, pressure and temperature variations in the shell side in axial direction, convective (estimated based on empirical correlations) and radiative heat transfer from the gas to the refractory lining and tubes outer surface according to equations (6)-(14) of the study by Hoseinzade et al.[27]
(3) outer tube wall of the mixed reforming tubes	Considers the temperature gradient in the axial and radial directions of the outer tube based on conductive heat transfer as given by equations (15)-(18) of the study by Hoseinzade et al.[27]
(4) gas phase in the reforming tubes	Considers the concentration, pressure (pressure drop was estimated based on Ergun equation) and temperature variations in the gas phase of the tubes in axial direction, convective heat transfer from the gas to the outer and inner tube walls and catalyst surface as given by equations (19)-(37) of the study by Hoseinzade et al.[27]
(5) catalyst particles	Considers temperature and concentration gradients within the catalyst particles, surface-to-gas mass and heat transfer, multi-species diffusion correlations, heat transfer correlations according to equations (38)-(43) of the study by Hoseinzade et al.[27] and reaction kinetics as given by equations (5)-(27) of section 2.1 of this work

(6) inner tube wall	Considers the temperature gradients in the axial and radial directions of the inner tube based on the conductive heat transfer correlation according to equations (64)-(67) of the study by Hoseinzade et al.[27]
(7) gas phase in the inner tubes	Considers the concentration, pressure and temperature gradients in the inner tube in axial direction, convective heat transfer from the gas to the inner tube inner surface according to equations (68)-(73) of the study by Hoseinzade et al.[27]

Table 2. Model assumptions.

Assumptions	Reference
Ideal gas law	28
Radial gradients in the reformer tubes are negligible	29
Conditions of one tube represent the other tubes as well	30
Heavier than methane hydrocarbons are converted in a pre-reformer, thus neglected from the model	31
Carbon deposition will not occur due to high steam to carbon ratio	2
Pressure drop in the shell and inner tube side is small and fixed at 1 bar	27, 32

2.1. Mixed reforming kinetics

The kinetic model of the combined reforming reaction is presented by Park et al.[18] for the Ni-based catalyst. As mentioned earlier, Park et al.[18] combined the kinetics provided by Xu and Froment[11], a well-known kinetic model for the SMR reaction, and the kinetic expression provided by Olsbye et al.[14] for the dry reforming process. The model is a Langmuir-Hinshelwood

type equation and Park et al. developed correlations for coefficients based on their experimental data. The reaction rates for equation (1)-(4) are given by equations (5)-(8), respectively.

$$r_1 = \frac{k_1[p_{CH_4}\, p_{H_2O} - \frac{p_{H_2}^3 p_{CO}}{K_1}]}{p_{H_2}^{2.5}\,(1+K_{CO}p_{CO}+K_{H_2}p_{H_2}+K_{CH_4}p_{CH_4}+\frac{K_{H_2O}p_{H_2O}}{p_{H_2}})^2} \quad (5)$$

$$r_2 = \frac{k_2[p_{CO}\, p_{H_2O} - \frac{p_{H_2} p_{CO_2}}{K_2}]}{p_{H_2}\,(1+K_{CO}p_{CO}+K_{H_2}p_{H_2}+K_{CH_4}p_{CH_4}+\frac{K_{H_2O}p_{H_2O}}{p_{H_2}})^2} \quad (6)$$

$$r_3 = \frac{k_3[p_{CH_4}\, p_{H_2O}^2 - \frac{p_{H_2}^4 p_{CO_2}}{K_3}]}{p_{H_2}^{3.5}\,(1+K_{CO}p_{CO}+K_{H_2}p_{H_2}+K_{CH_4}p_{CH_4}+\frac{K_{H_2O}p_{H_2O}}{p_{H_2}})^2} \quad (7)$$

$$r_4 = \frac{k_4[p_{CH_4}\, p_{CO_2} - \frac{p_{H_2}^2 p_{CO}^2}{K_4}]}{(1+K_{CO}p_{CO}+K_{CH_4}p_{CH_4})(1+K_{CO_2}p_{CO_2})} \quad (8)$$

Where $p_i = C_{cat,i} R T_{cat}$ is the partial pressure of the corresponding species (calculated by assuming the ideal gas law), $C_{cat,i}$ is the molar concentration of the component *i* on the catalyst surface, and T_{cat} is the catalyst temperature. k_1, k_2, k_3 and k_4 are the reaction coefficient and defined by:

$$k_1 = 4.72 \times 10^6 \exp\left(-\frac{232{,}477}{R}\left(\frac{1}{T_{cat}} - \frac{1}{1123.15}\right)\right), \frac{mol\ Pa^{0.5}}{g\ h} \quad (9)$$

$$k_2 = 1.06 \times 10^{-3} \exp\left(-\frac{71{,}537}{R}\left(\frac{1}{T_{cat}} - \frac{1}{1123.15}\right)\right), \frac{mol}{Pa\ g\ h} \quad (10)$$

$$k_3 = 1.89 \times 10^3 \exp\left(-\frac{267{,}760}{R}\left(\frac{1}{T_{cat}} - \frac{1}{1123.15}\right)\right), \frac{mol\ Pa^{0.5}}{g\ h} \quad (11)$$

$$k_4 = 2.91 \times 10^{-7} \exp\left(-\frac{234{,}851}{R}\left(\frac{1}{T_{cat}} - \frac{1}{1123.15}\right)\right), \frac{mol}{g\ h\ Pa^2} \quad (12)$$

The equilibrium constants are defined as:

$$\ln K_1 = 2.48 - \frac{22920.6}{T_{cat}} + 7.19 \ln T_{cat} - 2.95 \times 10^{-3} T_{cat} \quad (13)$$

$$\ln K_2 = -12.11 + \frac{5318.69}{T_{cat}} + 1.01 \ln T_{cat} + 1.14 \times 10^{-4} T_{cat} \quad (14)$$

$$K_3 = K_1 K_2 \quad (15)$$

$$K_4 = K_1/K_2 \quad (16)$$

Where the unit of K_1 is Pa^2 and K_2 is dimensionless. The adsorption coefficients are defined by:

$$K_{CH_4} = 6.65 \times 10^{-9} \exp\left(\frac{38{,}280}{R\,T_{cat}}\right), Pa^{-1} \quad (17)$$

$$K_{H_2O} = 1.77 \times 10^{5} \exp\left(-\frac{88{,}680}{R\,T_{cat}}\right) \quad (18)$$

$$K_{H_2} = 6.12 \times 10^{-14} \exp\left(\frac{82{,}900}{R\,T_{cat}}\right), Pa^{-1} \quad (19)$$

$$K_{CO} = 8.23 \times 10^{-10} \exp\left(\frac{70{,}650}{R\,T_{cat}}\right), Pa^{-1} \quad (20)$$

$$K_{CO_2} = 5.97 \times 10^{-7} \exp\left(\frac{52{,}670}{R\,T_{cat}}\right), Pa^{-1} \quad (21)$$

Based on the equations (1)-(4), reaction rates of the components can be written as:

$$r_{CH_4} = -(r_1 + r_3 + r_4) \quad (22)$$

$$r_{H_2O} = -(r_1 + r_2 + 2r_3) \quad (23)$$

$$r_{CO} = r_1 - r_2 + 2r_4 \quad (24)$$

$$r_{H_2} = 3r_1 + r_2 + 4r_3 + 2r_4 \quad (25)$$

$$r_{CO_2} = r_2 + r_3 - r_4 \quad (26)$$

$$r_{N_2} = 0 \quad (27)$$

The resulting model is a set of PDAEs which is implemented in the gPROMS software package[33]. The PDAEs are discretized in space using finite difference method. Also the grid size for the discretization in different axis is chosen based on reducing the global energy and mass conservations errors as described in the previous work.

3. Model validation

A survey in the literature shows there is no experimental data on the proposed integrated HTGR/MRM process to validate the model predictions. However, some lab scale experimental data on the mixed reforming process are available. As mentioned earlier, the model applied in

this study is an extension of the model developed in our previous work[27] to the mixed reforming process. The only difference of the models is the reaction kinetics applied for the tube side. The model of the integrated HTGR/SMR process was validated and fitted in the previous work and results demonstrated high accuracy of the model in predicting the reported design specifications. Since the shell side model is exactly the same in both models, it is necessary to validate the tube side model only.

Park et al. presented a kinetic model for the mixed reforming process and carried out experiments on the mixed reforming process for the equilibrium and non-equilibrium reactions[18, 34]. The results of these experiments are employed here to validate the tube side model. In the latest study by Park et al.[18], experiments were conducted for non-equilibrium reaction by adding diluents and decreasing the residence time of the components in the reactor. The experiment conditions are briefly described as follows: the fixed bed reforming reactor was embedded inside a heater such that the tube wall temperature was kept constant and equal to the temperature of the inlet process gas; the temperature in the study is in the range of 700-900º C, pressure is 0.5-1.2 MPa and GHSV is 90,000-280,000 mL-CH_4/g_{cat} h. The amount of the catalyst and diluent (α-Al_2O_3) used in the experiment were 50 mg and 1g, respectively. The steam to methane and carbon dioxide to methane ratios were kept constant at CO_2/CH_4=0.3 and H_2O/CH_4=1.7 in this experiment. Furthermore, in the experiment conditions, feed was flowing in the tube filled with catalyst and diluent particles, receiving heat from the heater and converted to the syngas, and then produced hot syngas leaving the tube. To simulate the experiment conditions, the inner tube sub-model is removed from the model. More details about the experiment conditions can be found in the study by Park et al.[18].

One of the significant differences between the experiment conditions and large scale design is the bed porosity. In the developed model for large scale systems, bed porosity was approximated using the given correlations in the literature for the fixed bed catalytic reactors based on the diameter of both the tube and catalyst particles[35]. However, in the experiment in order to prevent the reaction from reaching equilibrium, only small amount of catalyst was loaded in the reactor. By definition, bed porosity in packed bed reactors is the ratio of the free volume to the total volume of the reactor as follows:

$$\varepsilon_{cat} = 1 - \frac{V_p}{V_t} = 1 - \frac{m_p \rho_p}{\pi D_t^2 L/4} \quad (28)$$

Where, ε_{cat} is the bed porosity with respect to the catalyst particles which is used to compute the catalyst surface area ($a_v = 6(1-\varepsilon_{cat})/D_p$), V_p is the volume occupied by the catalyst particles, m_p is the net weight of the catalyst loaded, ρ_p is the particle density, V_t is the reactor volume, D_t is the reactor inner diameter (10.9 mm) and L is the reactor length (6 mm). The reactor diameter and length were not reported in the article, but were provided by the authors via email[36]. The only parameter fitted for model validations is the catalyst particle size within a tight range known from Park study[18].

In those experiments, a portion of the reactor volume was occupied by diluent particles ($\alpha - AL_2O_3$ balls) to control the mixed reforming reaction progress. There is no reaction on the diluent particles, however, it affects the velocity and pressure drop of the gas stream flowing in the reactor. Therefore, the bed porosity definition was adjusted in the model to reflect the experimental setup, defining it as ratio of the free volume to the reactor volume:

$$\varepsilon_t = 1 - \frac{V_p + V_d}{V_t} = 1 - \frac{m_p\rho_p + m_d\rho_d}{\pi D_t^2 L/4} \quad (29)$$

Where ε_t is the bed porosity considering any particles, V_d is the volume of the diluent particles, m_d is the net weight and ρ_d is the density of the diluent particles.

With these assumptions, the results of the model prediction at different temperatures, pressures and GHSVs are shown in figure 2. In the figure, the model predictions are shown as red lines and the experimental data with the black circles. The base condition for the experiments is GHSV=180,000 mL-CH_4/g_{cat} h, a temperature of 800º C and a pressure of 1.0 MPa. At each series of experiments one of these operating conditions was perturbed from the base condition.

It should be noted that GHSV is measured at the standard temperature and pressure (STP) condition[18] and converted to the methane molar flow rate ($\dot{F}_{CH_4}$) by the following equation:

$$\dot{F}_{CH_4} = \frac{GHSV \times m_p \times P_{STP}}{RT_{STP}Z_{STP}} \quad (30)$$

Where, P_{STP} is the pressure, T_{STP} is the temperature and Z_{STP} is the methane compressibility factor at the STP condition.

The system performance is shown by variations of the methane and carbon dioxide conversions and the hydrogen to carbon monoxide ratio (H_2/CO) as it is used in Park's study. The results

indicate that at each data point, tube model can predict methane and carbon dioxide conversions and the H_2/CO ratio with high accuracy. The average absolute error in the CO_2 and methane conversions and H_2/CO ratio predictions is 2%, 4.35% and 0.183, respectively. It should be noted that presented model indicates better agreement with the experimental data than the simulation results in the Park study[18]. This is because the presented model considers more detailed phenomena, such as multi-species diffusion correlations[37], temperature and concentration variations in the catalyst phase as well as heat transfer coefficients and so on. Validating the model in the non-equilibrium condition and with only a single parameter fitting means that all of the correlations applied for the diffusion, heat transfer coefficient, reaction kinetics, physical properties as well as assumptions made to develop the model are valid and can be used for the large scale design.

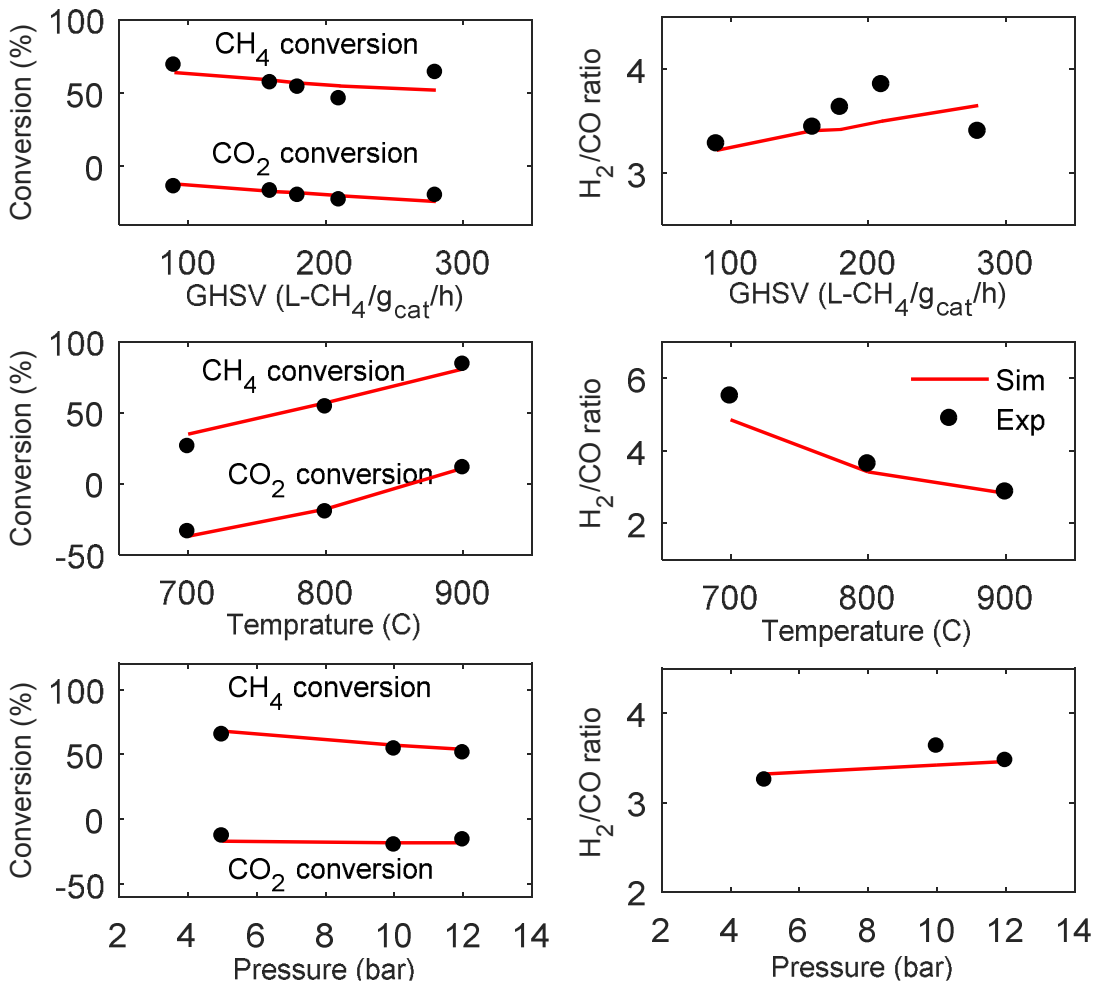

Figure 2. Model validation at non-equilibrium conditions. Experimental data was derived from the Park study[18].

In addition, the tube model is validated using other experimental data sets reported by Jun et al.[34] at equilibrium and non-equilibrium conditions. In this data set, 9 cases were studied at equilibrium conditions (cases 1-9 of the study by Jun et al.[34]) and 8 cases at non-equilibrium conditions (cases 10-17 of the study by Jun et al.[34]). Similar to the previous case, the fixed bed reactor is embedded inside a heater to keep the tube wall temperature constant, which we replicated in our model for validation purposes by fixing the boundary condition of the inner tube wall temperature accordingly. The temperature in the experiment was in the range of 700-900º C, pressure was 0.25-1.0 MPa, GHSV was 2500-400,000 mL-CH_4/g_{cat} h and molar ratios are $CH_4/CO_2/H_2O/N_2$=3/1-1.2/2-4/3-4. The reactor inner diameter is 10 mm and the length is 30 mm. More details about the experiments can be found in the study by Jun et al.[34].

With the given conditions, model predictions and experimental data for the equilibrium and non-equilibrium conditions of methane and carbon dioxide conversions are indicated in figure 3. The identity line shown with dashes in Figure 3 clearly demonstrates that the deviation of model predictions from experimental data is low. In the experiments, in order to reach equilibrium, the space velocity of inlet gas was kept low such that sufficient residence time was given for the reactants to reach equilibrium. Figure 3.a shows that in many cases methane equilibrium conversion is slightly underestimated by the model, and the average absolute error of prediction is 6.59%. However, as shown by Figure 3.b, the equilibrium conversion of CO_2 and model prediction are close and the average absolute error of the prediction is 3.1%.

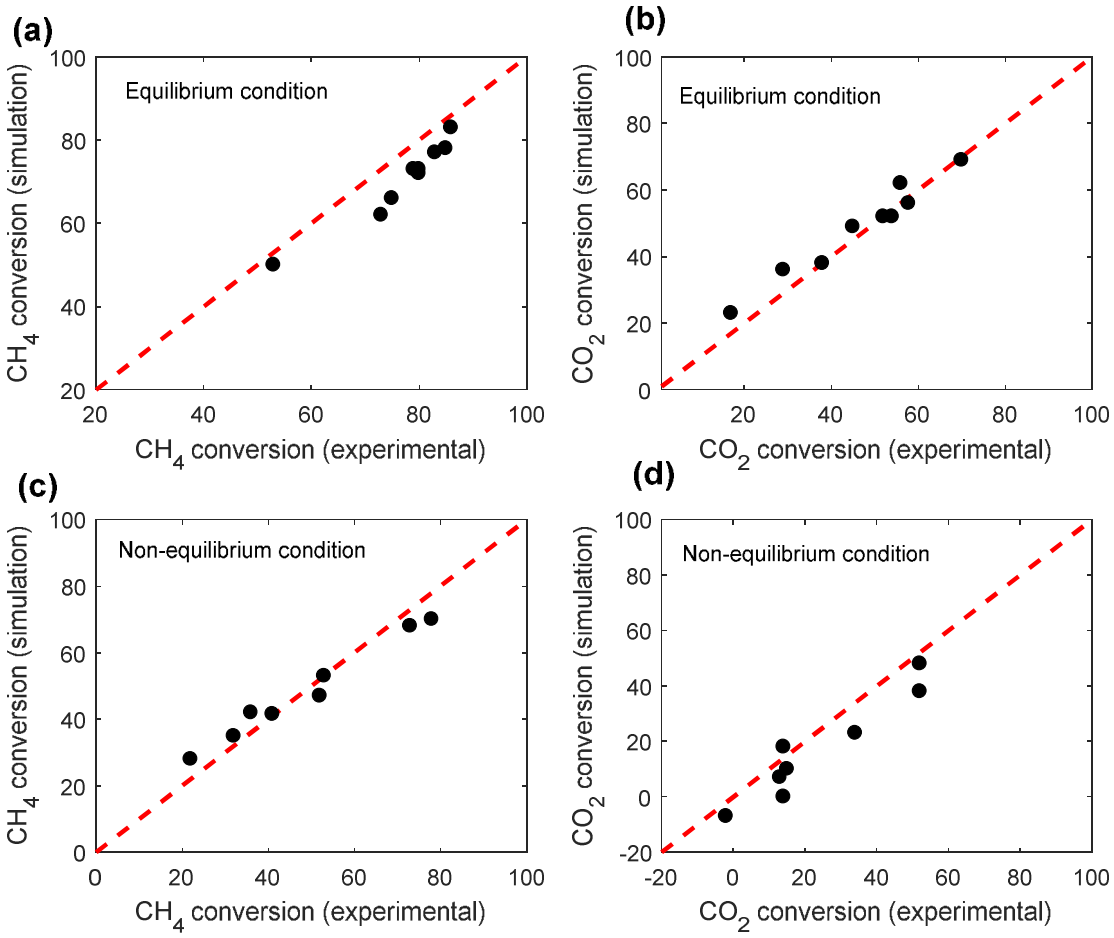

Figure 3. Parity plots of the experimental and simulation results for the methane and CO_2 conversions at equilibrium and non-equilibrium conditions. Experimental data was derived for cases 1-17 from figure 2 of the study by Jun et al.[34].

Figure 3.c and d indicate the model prediction and experimental data for non-equilibrium data set (cases 10-17 of the study by Jun et al.[34]). The non-equilibrium condition in experiments was attained by increasing the feed flow rate up to eighty times from the equilibrium condition, and by adding some diluent solids (alumina balls). The operating conditions for each case is given in the study by Jun et al.[34]. The system behavior is shown by variations of the methane and carbon dioxide conversions for this data set. The results depict that for all cases, tube model compares well methane and carbon dioxide conversions to the experimental results. The average absolute error in the CO_2 and methane conversions are 4.2% and 7.8%, respectively.

4. Results and discussion

The objective of this section is to present an analysis of a large scale design for the proposed integrated HTGR/MRM system. SIEMENS-INTERATOM provided a large scale design for the integrated HTGR/SMR system for hydrogen production[21]. The operating conditions of the presented design are extended from this reference to the integrated HTGR/MRM system. Since the DRM reaction is more endothermic than SMR, a lower process gas feed rate (or a higher helium feed rate) is required to obtain the same cooling duty as the SMR process studied in the previous work[27]. Therefore, a lower process gas (mixture of methane, steam and carbon dioxide) feed rate is required in the MRM process to obtain the same cooling duty as the SMR-only process.

It can be challenging to choose optimal steam to methane and CO_2 to methane ratios in the MRM process. For example, due to the presence of CO_2, carbon deposition is possible which depends on the steam to methane and CO_2 to methane ratios as well as the type of catalyst[2]. These ratios also affect the heat duties, heat transfer properties, conversion rates, and outlet gas concentrations, all of which have impacts both on the equipment design and on the balance-of-plant. A survey of the literature shows that different ratios are applied depending on the application of syngas in the downstream; however, there is a carbon limit for the H_2O/CH_4 and CO_2/CH_4 ratios for certain types of catalyst[2]. The selected ratios in this study has been derived from the industrial reported data in[2]. Based on the carbon limit diagram provided in[2], the ratios chosen for this work are located in the safe region (no carbon deposition region) for the Ni-based catalyst. Furthermore, the design parameters are taken from either the SIEMENS-INTERATOM design or the fitted parameters in our previous study[27]. The operating conditions and design parameters used for the large scale HTGR/MRM process are given in Tables 3 and 4, respectively.

Table 3. Design specification for the industrial scale integrated system.

Specification		Large scale design
Process gas conditions		
Inlet pressure[21]		5.6 MPa
Inlet temperature[21]		347ºC
Feed rate		30.8 mol/hr.tube
Methane/Steam/CO_2	ratio	1/2.5/1.5
[Mortensen]		
Helium gas conditions[21]		

Inlet pressure	4.987 MPa
Inlet temperature	950ºC
Feed rate	50.3 kg/s

Table 4. Design parameters[21, 27].

Parameter	Value
Number of tubes	199
Catalyst type	Ni-Alumina
Tube material	Incoloy 617
Tube length	14 (m)
Tube wall thickness	1 (cm)
Tube inner outer diameter	12 (cm)
Inner tube thickness	0.165 (cm)
Inner tube inner diameter	5.72 (cm)
Refractory inner diameter	2.7 (m)
Inner tube material	Alloy IN 519

Based on the design specifications and parameters in Tables 3 and 4, the system behavior is analyzed in this section. The final model implemented in gPROMS contains 233,538 variables. To initialize the simulations in gPROMS, all tube side gases (including within the catalyst particles) were set at time zero to be pure nitrogen at 620.15K, with the inlet to the tubes also pure nitrogen at 620.15K and 56 bar. Similarly, the shell side was set to be pure helium at 620.15K, with the inlet to the shell at 620.15K and 49.87 bar. This created a set of initial conditions that was consistent with the model equations and thus allowed the simulation to initialize. Then, the simulation was run until a steady state was attained. Then, the inlet stream conditions were changed to those given in Table 3 and the dynamic simulation was continued until a new steady state condition was obtained. This new steady state condition was saved for use as a set of consistent initial conditions for use in all future simulations, and all previous time steps were discarded.

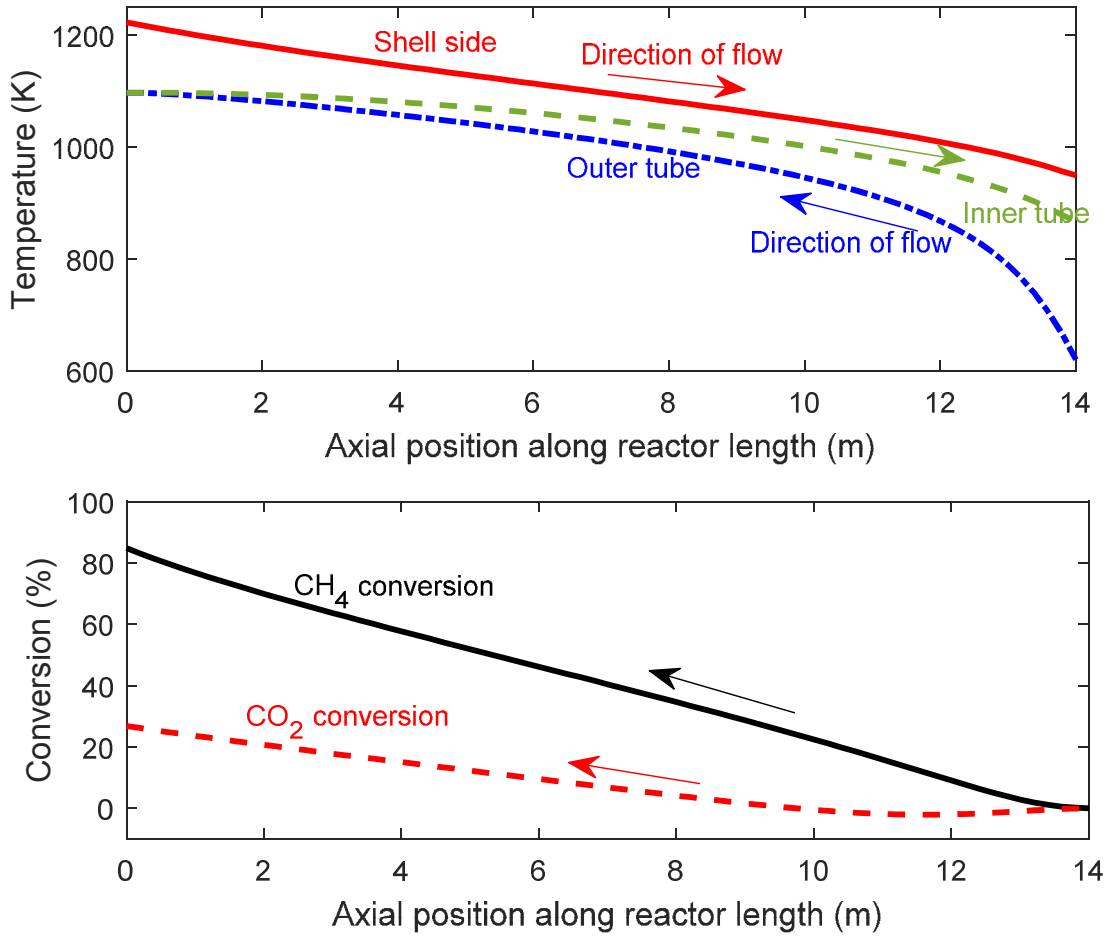

Figure 4. Temperatures and conversions profiles at the steady state conditions.

The steady state performance of the integrated HTGR/MRM system is shown in Figure 4 as a function of axial position of the shell, outer tube, and inner tube gas phase temperatures, methane and CO_2 conversions in the outer tube section. Figure 4 shows that helium gas in the shell side transfers heat to the tube wall and its temperature decreases from 1223.15 K to 949.6 K with a corresponding cooling duty of 72 MW. In the outer tube, process gas receives heat through the outer tube and inner tube walls, converted to the syngas and its temperature increases from 620.15 K to 1159.1 K; then the hot syngas proceeds in the inner tube to transfer its heat to the tube side such that its temperature drops from 1159.1 K to 867.2 K. Also, the overall methane and CO_2 conversions are 84.8% and 26.9%, respectively. The CO_2 conversion is low due to the high pressure of the feed. One solution to increase CO_2 conversion at the systems level is to separate unreacted CO_2 from the product and recycle that to the system. In addition, the syngas outlet has an H_2/CO ratio of 1.7. In order to reach higher H_2/CO ratios, extra steam is required.

Further analysis found that in order to achieve an H_2/CO ratio of 2 at the given operating conditions in Table 1, $CH_4/H_2O/CO_2$ feed ratios of 1/3.4/1.5 is required.

The results show that methane conversion is significantly higher in this system than the integrated SMR/HTGR system (without DRM). In addition to higher methane conversion, 26.9% of the CO_2 converted to syngas. However, in the SMR-only process some CO_2 is produced during the reaction. This demonstrates the potential for lower GHG emissions of the integrated reforming/HTGR systems by combining steam and dry reforming processes, although a rigorous life cycle analysis in the context of the balance-of-plant is a subject of future work.

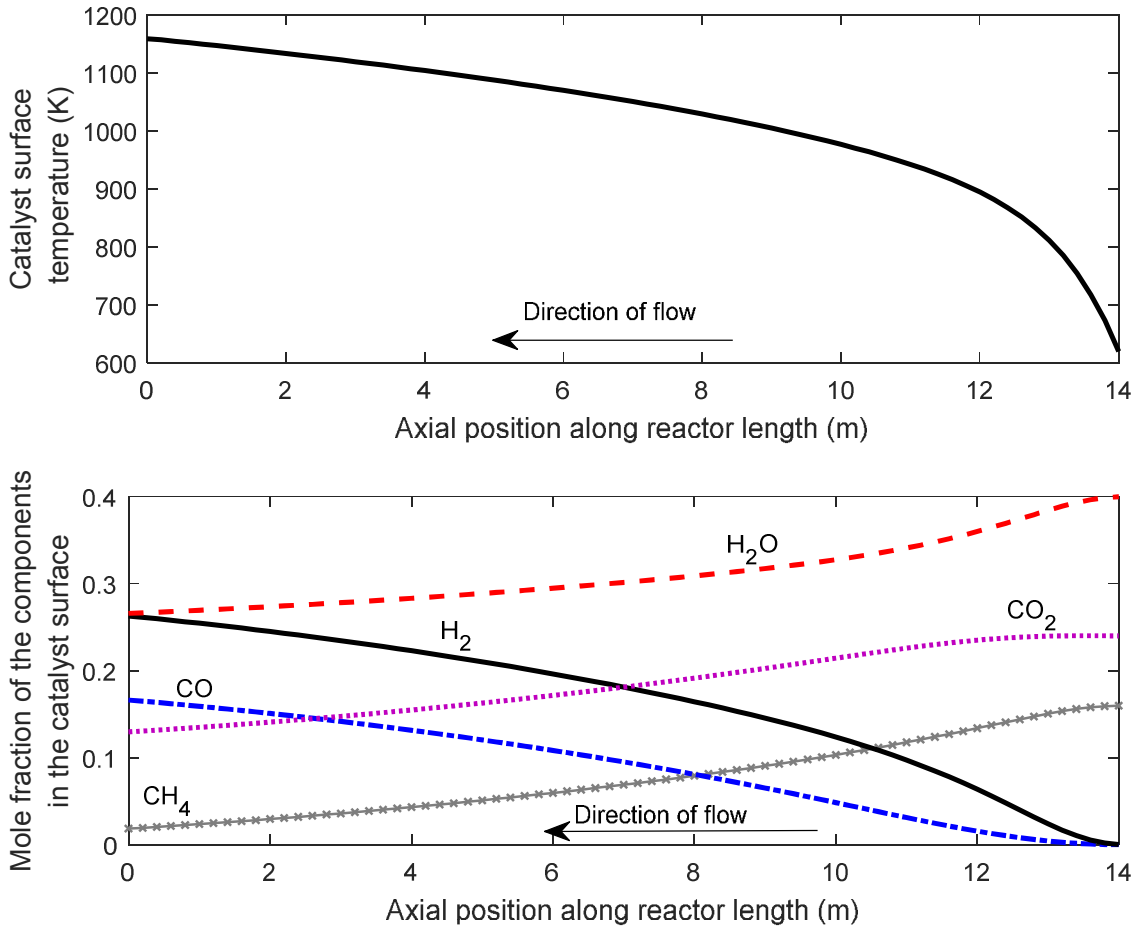

Figure 5. Temperature and mole fraction profiles in the catalyst surface at steady state condition.

Figure 5 shows the steady state temperature in the catalyst surface as a function of axial position. Based on the results, the catalyst surface temperature reaches to 1158.0 K in the outer tube outlet which is very close to the syngas temperature in the outer tube outlet. Furthermore, figure 5 shows the mole fraction profile of the components in the catalyst surface at steady state. The

profiles indicate that methane is consumed faster than steam and carbon dioxide within the reactor length. Similarly, the hydrogen production rate is faster than that of carbon monoxide, which leads to a H_2/CO ratio of 1.7. In addition, the results show that more than half of the steam and CO_2 leave the reforming tubes unreacted.

4.2.Effect of disturbances

In this section, the impact of the disturbances on the inlet helium or process gas (methane, steam and CO_2 mixture) feed such as disturbances in the helium and process gas inlet temperatures is presented. The first disturbance studied is a step change of +50 K in the helium gas feed temperature from steady state. As a result of this change, the shell and inner tube outlet temperatures as well as the methane and CO_2 conversions significantly increased. Figure 6 indicates the response of the key variables of the system at the exit (z=14 m) to this change. As shown in the figure, the steady state value of the shell exit temperature increased from 949.6 K to 971.8 K which resulted in a cooling duty increase of 7.3 MW. The inner tube outlet temperature increased from 867.2 K to the new steady state of 884.1 K; Methane and CO_2 conversions also significantly increased and reached new steady state values of 95.3% and 34.1%, respectively. It can be concluded from the results that helium gas inlet temperature changes remarkably affect the key variables of the system.

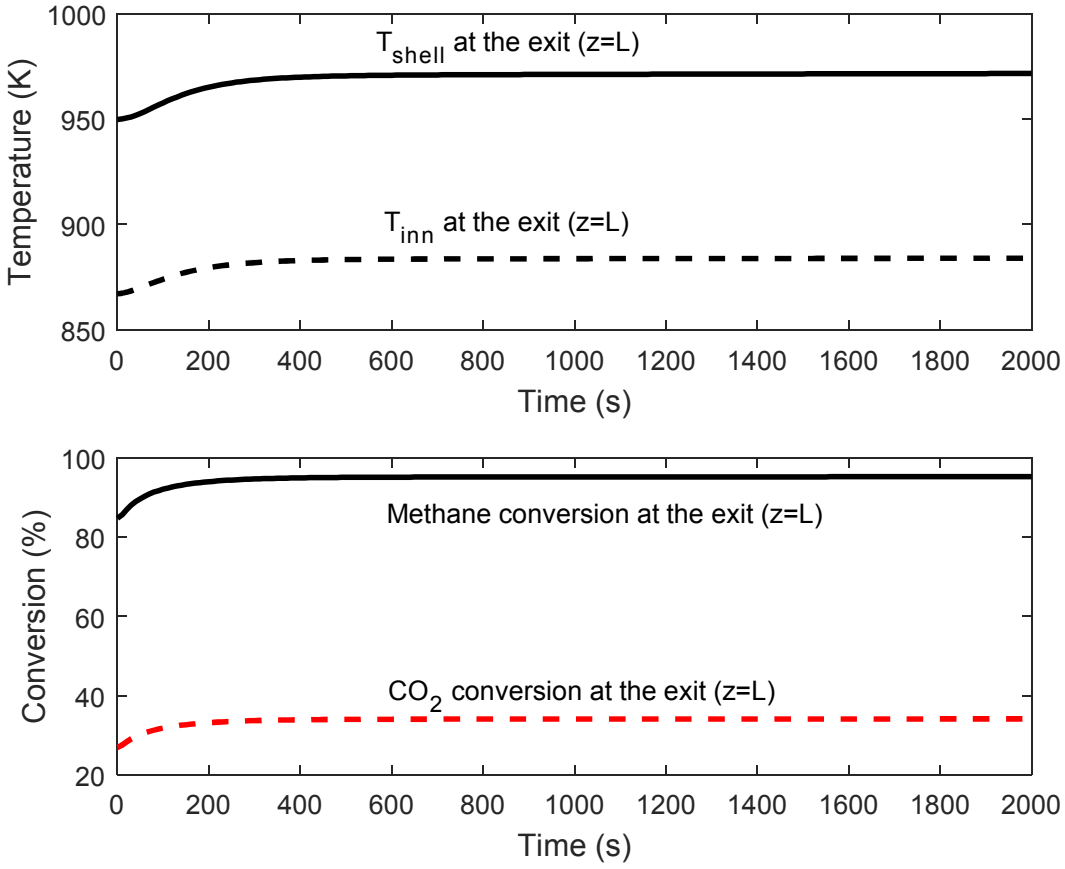

Figure 6. Effect of 50 K increase in the helium gas feed at t=0 (s) on the outlet temperatures of the shell and inner tube gases and conversions of methane and CO_2.

The second disturbance investigated here is a 50 K increase in the process gas inlet feed temperature. Figure 7 shows the impact of this change on the shell and inner tube exit temperatures as well as the methane and carbon dioxide conversions in the outlet. As a result of this change, shell outlet temperature increased from the 949.6 K to the new steady state of 958.4 K, resulting in a decrease in the cooling duty of the system to 69.2 MW. In the inner tube side, syngas exit temperature increased from 867.2 K to 881.8 K. Methane conversion went up only by 0.7 percentage points, and CO_2 conversion only increased by 0.2 percentage point. The results show that disturbances in the process gas inlet temperature have insignificant impact on the system performance.

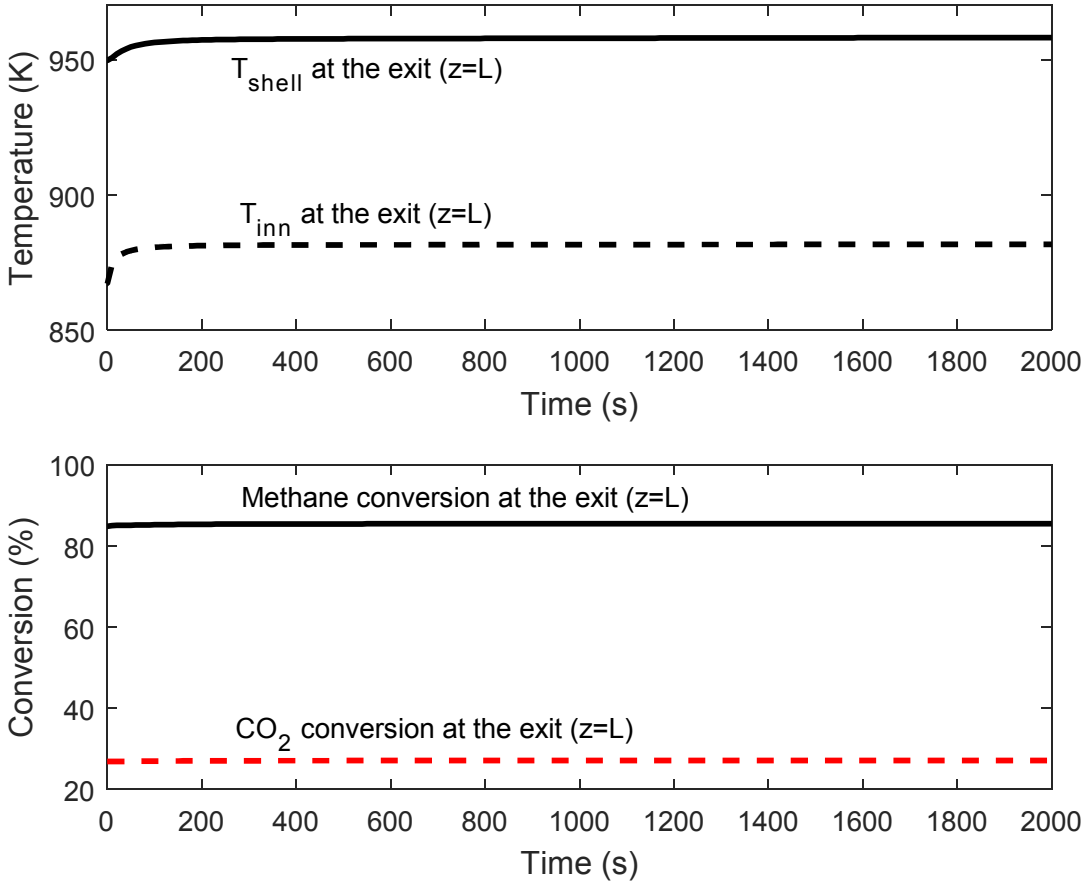

Figure 7. Effect of 50 K increase in the process gas feed at t=0 (s) on the outlet temperatures of the shell and inner tube gases and conversions of methane and CO_2.

4.2.Sensitivity analysis

In this section, the impact of key design parameters on performance of the system is presented. Although the given parameters reported in Table 4 are the design data from the literature, it is

necessary to determine the key parameters of the system and investigate the impact of those on the system performance. The sensitivity of the system to uncertain parameters was analyzed for 5% and 10% changes in the base value of the inner tube diameter, catalyst particle size and tube length. The key design variables to represent the performance of the system are the shell exit temperature, the cooling duty of the system, and the methane and CO_2 conversions. Figure 8 shows the percentage of change from the base case values by ±5% and ±10% changes in the base values of the parameters given in Table 4.

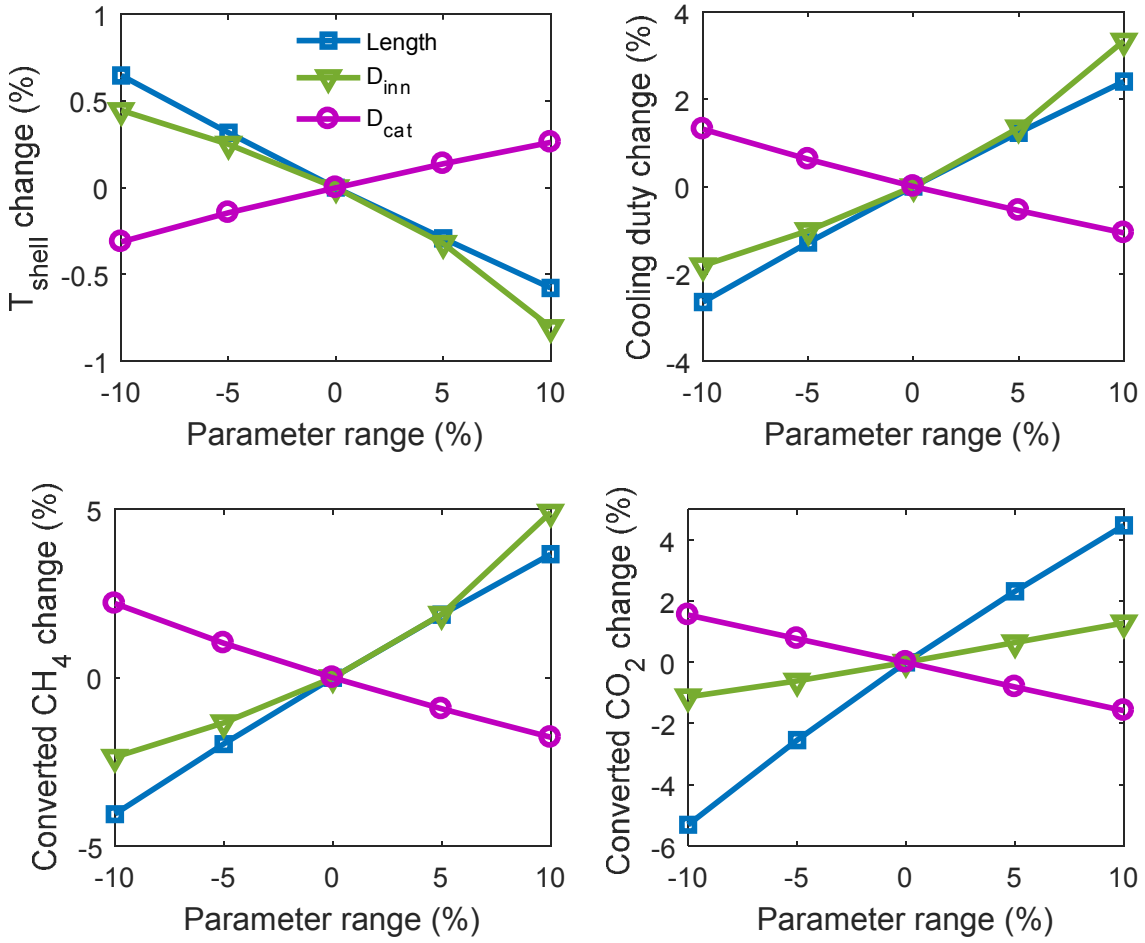

Figure 8. Sensitivity of exit temperatures of the shell, CH_4 and CO_2 exit conversions and cooling duty of the system to some of the model parameters (tube length, outer and inner diameters of the inner tube, and catalyst diameter).

This figure indicates that as a result of a ±10% change in the value of the parameters, shell exit temperature shows a maximum change of ±0.8%. This shows that shell outlet temperature is not very sensitive to the parameter uncertainty. The cooling duty is moderately sensitive to parameter changes. The maximum change of the cooling duty is 3.3% from a 10% increase in the

inner and outer diameter of the inner tube. The methane and carbon dioxide conversions are more sensitive to parameter changes. As a result of ±10% change in the parameters, the moles of converted methane and carbon dioxide change ±4.9% and ±5.3%, respectively. This shows that for the case of 10% parameter uncertainty, the maximum change in the key variables of the system is 5.3% which is still small and implies that system performance is not very sensitive to the parameter uncertainty.

In all the cases, the catalyst particle diameter is the least influential parameter. However, the impact of the tube length and the inner tube diameter is stronger. It can be concluded from the figure that despite the inner tube diameter, tube length affects the system performance roughly linearly. The results show that increasing the inner tube diameter improves the conversions and the cooling duty of the system. This is due to an increase in the heat transfer from the inner tube to the tube. However, increasing the inner tube diameter also leads to the higher pressure drop in the tube side. The same explanation applies for the tube length as well. In addition, increasing the tube length increases the conversions and cooling duty, but it does not mean longer tubes are necessarily optimal due to pressure drops and capital cost limits. Therefore, the optimal values of these parameters must be determined at the systems level depending on how the HTGR/MRM is used.

5. Conclusions

This study presented a dynamic two-dimensional and multi-scale model for the integrated HTGR/MRM process for syngas production. The model was extended from the previous work by Hoseinzade and Adams[27] to this study. The model is based on first principles and well-known empirical correlations for physical properties, diffusion, heat and mass transfer coefficients and reaction kinetics. Due to lack of experimental data on the integrated HTGR/MRM process, the model was validated for the tube side only using the reported experimental data. The shell side model was already validated in the previous study. The developed model for the mixed reforming reactor was validated using over 25 experimental data points for equilibrium and non-equilibrium reactions at steady state conditions. The results demonstrate that the model predicts experimental data extremely well either in equilibrium or non-equilibrium conditions. The model of integrated HTGR/MRM system was re-applied to commercial scales using design criteria presented in the literature, and used that to predict key performance criteria such as methane and

CO_2 conversions. It has been demonstrated that integrating nuclear heat with the mixed reforming process is a promising, option to achieve H_2/CO ratios suitable for FT processes. Furthermore, the most important design parameters were identified to be the tube length and the inner tube diameter from a sensitivity analysis, which will help in the design of other HTGR/MRM systems for different applications.

The HTGR/MRM process has potential to be applied in many types of energy conversion systems, such as converting natural gas and nuclear energy into synthetic fuels. Therefore, the presented model is useful to address the key challenges of any applications of integrated HTGR/MRM systems. The inclusion of DRM has the capability to consume CO_2 as a reagent. Thus, depending on the design objectives and how the HTGR/MRM system is integrated with the balance of plant, there is the possibility that it would result in lower lifecycle GHG emissions than using an HTGR/SMR and especially a SMR only approach. The presented model provides the possibility to answer the questions on the life cycle impacts of HTGR/MRM system. However, analyzing the life cycle of the HTGR/MRM systems in various usage cases is the subject of future study.

Acknowledgment

Financial support from the Ontario Ministry of Innovation via Early Researcher Award ER13-09-213 with matching support from the McMaster Advanced Control Consortium is gratefully acknowledged.

Nomenclature

Subscripts

r	Reaction
p	Particles
d	Diluent
$shell$	Shell
w	Tube wall
w_2	Inner tube wall
gas	Mixture of gases in the tube
cat	Catalyst phase
i	Component counter

t	Tube
inn	Inner tube gas

Acronyms

SMR	Steam methane reforming
DRM	Dry reforming of methane
MRM	Mixed reforming of methane
FT	Fischer-Tropsch
POM	Partial oxidation of methane
HTGR	High temperature gas-cooled reactor
WGS	Water gas shift
GHSV	Gas hourly space velocity
GHG	Greenhouse gases
PDAE	Partial differential algebraic equation
STP	Standard temperature and pressure

Greek letters

ρ	Density
ε	Bed porosity
π	mathematical constant
κ	Mass transfer coefficient

References

(1) Rostrup-Nielsen, J. R. Syngas in perspective. *Catal. Today*. **2002**, *71*(3), 243.

(2) Mortensen, P. M.; Dybkjær, I. Industrial scale experience on steam reforming of CO_2-rich gas. *Appl. Catal. , A*. **2015,** *495*, 141.

(3) Abashar, M. E. E. Coupling of steam and dry reforming of methane in catalytic fluidized bed membrane reactors. *Int. J. Hydrogen Energy*. **2004,** *29*(8), 799.

(4) O'Connor, A. M.; Schuurman, Y.; Ross, J. R.; Mirodatos, C. Transient studies of carbon dioxide reforming of methane over Pt/ZrO_2 and Pt/Al_2O_3. *Catal. Today*. **2006,** *115*(1), 191.

(5) Chen, J.; Wang, R.; Zhang, J.; He, F.; Han, S. Effects of preparation methods on properties of $Ni/CeO_2–Al_2O_3$ catalysts for methane reforming with carbon dioxide. *J. Mol. Catal. A: Chem.***2005,** *235*(1), 302.

(6) Sadykov, V. A.; Gubanova, E. L.; Sazonova, N. N.; Pokrovskaya, S. A.; Chumakova, N. A.; Mezentseva, N. V.; Bobin, A. S.; Gulyaev, R. V.; Ishchenko, A. V.; Krieger, T. A.; Mirodatos, C. Dry reforming of methane over Pt/PrCeZrO catalyst: kinetic and mechanistic features by transient studies and their modeling. *Catal. Today.* **2011,** *171*(1), 140.

(7) Richardson, J. T.; Paripatyadar, S. A. Carbon dioxide reforming of methane with supported rhodium. *Appl. Catal.***1990,** *61*(1), 293.

(8) Rostrupnielsen, J. R.; Hansen, J. B. CO_2-reforming of methane over transition metals. *J. Catal.* **1993,** *144*(1), 38.

(9) Wang, S.; Lu, G. Q.; Millar, G. J. Carbon dioxide reforming of methane to produce synthesis gas over metal-supported catalysts: state of the art. *Energy Fuels.* **1996,** *10*(4), 896.

(10) Elnashaie, S. S. *Modelling, simulation and optimization of industrial fixed bed catalytic reactors*; CRC Press, 1994.

(11) Xu J.; Froment G. F. Methane steam reforming, methanation and water-gas shift: I. Intrinsic kinetics. *AIChE J*. **1989**, *35*(1), 88.

(12) Bradford, M. C.; Vannice, M. A. Catalytic reforming of methane with carbon dioxide over nickel catalysts I. Catalyst characterization and activity. *Appl. Catal. , A*. **1996**, *142*(1), 73.

(13) Bradford, M. C.; Vannice, M. A. Catalytic reforming of methane with carbon dioxide over nickel catalysts II. Reaction kinetics. *Appl. Catal. , A*. **1996**, *142*(1), 97.

(14) Olsbye, U.; Wurzel, T.; Mleczko, L. Kinetic and reaction engineering studies of dry reforming of methane over a $Ni/La/Al_2O_3$ catalyst. *Ind. Eng. Chem. Res.* **1997**, *36*(12), 5180.

(15) Wang, S.; Lu, G. Q.. A comprehensive study on carbon dioxide reforming of methane over $Ni/\gamma\text{-}Al_2O_3$ catalysts. *Ind. Eng. Chem. Res*. **1999**, *38*(7), 2615.

(16) Maestri, M.; Vlachos, D. G.; Beretta, A.; Groppi, G.; Tronconi, E. Steam and dry reforming of methane on Rh: Microkinetic analysis and hierarchy of kinetic models. *J. Catal.* **2008**, *259*(2), 211.

(17) Zhao, Y. R.; Latham, D. A.; Peppley, B. A.; McAuley, K. B.; Wang, H.; LeHoux, R. Simulation of dry reforming of methane in a conventional downfired reformer. *AIChE J.* **2017**, *63*(6), 2060.

(18) Park, N.; Park, M. J.; Baek, S. C.; Ha, K. S.; Lee, Y. J.; Kwak, G.; Park, H. G.; Jun, K. W. Modeling and optimization of the mixed reforming of methane: maximizing CO_2 utilization for non-equilibrated reaction. *Fuel.* **2014**, *115*, 357.

(19) Larentis, A. L.; De Resende, N. S.; Salim, V. M. M.; Pinto, J. C. Modeling and optimization of the combined carbon dioxide reforming and partial oxidation of natural gas. *Appl. Catal. , A.* **2001**, *215*(1), 211.

(20) Koh, A. C.; Chen, L.; Leong, W. K.; Johnson, B. F.; Khimyak, T.; Lin, J. Hydrogen or synthesis gas production via the partial oxidation of methane over supported nickel–cobalt catalysts. *Int. J. Hydrogen Energy.* **2007**, *32*(6), 725.

(21) Yan, X. L.; Hino, R. *Nuclear hydrogen production handbook*. CRC Press, 2011.

(22) Inagaki, Y.; Nishihara, T.; Takeda, T.; Hada, K.; Ogawa, M.; Shiozawa, S.; Miyamoto, Y. Development programme on hydrogen production in HTTR. *No. IAEA-TECDOC--1210*. **2001**, 213.

(23) Fedders, H.; Harth, R.; Höhlein, B. Experiments for combining nuclear heat with the methane steam-reforming process. *Nucl Eng Des.* **1975**, *34*(1), 119.

(24) Höhlein, B.; Niessen, H.; Range, J.; Schiebahn, H. J.; Vorwerk, M. Methane from synthesis gas and operation of high-temperature methanation. *Nucl Eng Des*. **1984**, *78*(2), 241.

(25) Khojasteh Salkuyeh, Y.; Adams II, T. A. Combining coal gasification, natural gas reforming, and external carbonless heat for efficient production of gasoline and diesel with CO_2 capture and sequestration. *Energy Convers. Manage.* **2013**, *74*, 492.

(26) Khojasteh Salkuyeh, Y.; Adams II, T. A. A new power, methanol, and DME polygeneration process using integrated chemical looping systems. *Energy Convers. Manage*. **2014**, *88*, 411.

(27) Hoseinzade, L.; Adams II T. A. Modeling and simulation of the integrated steam reforming and nuclear heat systems. *Int. J. Hydrogen Energy*. **2017**, DOI:10.1016/j.ijhydene.2017.08.031.

(28) Adams II, T. A.; Barton, P. I. A dynamic two-dimensional heterogeneous model for water gas shift reactors. *Int. J. Hydrogen Energy.* **2009**, *34*(21), 8877.

(29) Nandasana, A. D.; Ray, A. K.; Gupta, S. K. Dynamic model of an industrial steam reformer and its use for multiobjective optimization. *Ind. Eng. Chem. Res.* **2003**, *42*(17), 4028.

(30) Pantoleontos, G.; Kikkinides, E. S.; Georgiadis, M. C. A heterogeneous dynamic model for the simulation and optimisation of the steam methane reforming reactor. *Int. J. Hydrogen Energy*. **2012**, *37*(21), 16346.

(31) Dybkjær, I. Tubular reforming and autothermal reforming of natural gas-an overview of available processes. *Fuel Process. Technol*. **1995**, *42*(2-3), 85.

(32) Ghouse, J. H.; Seepersad, D.; Adams II, T. A. Modelling, simulation and design of an integrated radiant syngas cooler and steam methane reformer for use with coal gasification. *Fuel Process. Technol*. **2015,** *138*, 378.

(33) gPROMS. *Process Systems Enterprise*, 2011.

(34) Jun, H. J.; Park, M. J.; Baek, S. C.; Bae, J. W.; Ha, K. S.; Jun, K. W. Kinetics modeling for the mixed reforming of methane over Ni-CeO_2/$MgAl_2O_4$ catalyst. *J. Nat. Gas Chem.* **2011,** *20*(1), 9.

(35) Francesconi, J. A.; Mussati, M. C.; Aguirre, P. A. Analysis of design variables for water-gas-shift reactors by model-based optimization. *J. Power Sources.* **2007**, *173*(1), 467.

(36) Park, M. J. Personal communication. **2017**, Feb 13.

(37) Ghouse, J. H.; Adams II, T. A. A multi-scale dynamic two-dimensional heterogeneous model for catalytic steam methane reforming reactors. *Int. J. Hydrogen Energy*. **2013**, *38*(24), 9984.

Abstract Graphic: